Mon. Not. R. Astron. Soc. **000**, 000–000 (0000) Printed 10 February 2015 (MN LATEX style file v2.2)

Discovery of a Shell of Neutral Atomic Hydrogen Surrounding the Carbon Star IRC+10216

L. D. Matthews[1], E. Gérard[2], T. Le Bertre[3]
[1] *Massachusetts Institute of Technology Haystack Observatory, Off Route 40, Westford, MA 01886 USA*
[2] *GEPI, UMR 8111, Observatoire de Paris, 5 Place J. Janssen, F-92195 Meudon Cedex, France*
[3] *LERMA, UMR 8112, Observatoire de Paris, 61 av. de l'Observatoire, F-75014 Paris, France*

10 February 2015

ABSTRACT

We have used the Robert C. Byrd Green Bank Telescope to perform the most sensitive search to date for neutral atomic hydrogen (H I) in the circumstellar envelope (CSE) of the carbon star IRC+10216. Our observations have uncovered a low surface brightness H I shell of diameter $\sim 1300''$ ($\sim$0.8 pc), centered on IRC+10216. The H I shell has an angular extent comparable to the far ultraviolet-emitting astrosphere of IRC+10216 previously detected with the *GALEX* satellite, and its kinematics are consistent with circumstellar matter that has been decelerated by the local interstellar medium. The shell appears to completely surround the star, but the highest H I column densities are measured along the leading edge of the shell, near the location of a previously identified bow shock. We estimate a total mass of atomic hydrogen associated with IRC+10216 CSE of $M_{\rm HI} \sim 3 \times 10^{-3}$ $M_{\odot}$. This is only a small fraction of the expected total mass of the CSE (<1%) and is consistent with the bulk of the stellar wind originating in molecular rather than atomic form, as expected for a cool star with an effective temperature $T_{\rm eff} \lesssim$2200 K. H I mapping of a $2^{\circ} \times 2^{\circ}$ region surrounding IRC+10216 has also allowed us to characterize the line-of-sight interstellar emission in the region and has uncovered a link between diffuse FUV emission southwest of IRC+10216 and the Local Leo Cold Cloud.

Key words: stars: AGB and post-AGB – stars: carbon – stars: fundamental parameters – circumstellar matter — stars: individual: IRC+10216 — ISM: clouds

1 INTRODUCTION

At a distance of ∼130 pc, IRC+10216 (CW Leonis) is the nearest example of a carbon-rich asymptotic giant branch (AGB) star. IRC+10216 is believed to be nearing the end of its evolution on the AGB and to be close to transitioning into a protoplanetary nebula (e.g., Skinner et al. 1998; Osterbart et al. 2000). Its proximity and advanced evolutionary state make IRC+10216 an object of considerable interest for understanding the late stages of evolution for intermediate mass stars. Some fundamental properties of IRC+10216 are summarized in Table 1.

As expected for a star approaching the end of its AGB lifetime, IRC+10216 is undergoing mass loss at a high rate ($\sim 2 \times 10^{-5}$ $M_{\odot}$ yr^{-1}) and is surrounded by an extensive circumstellar envelope (CSE). This CSE has been widely studied using a variety of observational tracers, including dust-scattered optical light (Mauron & Huggins 1999); far infrared emission from dust (e.g., Young et al. 1993; Ladjal et al. 2010; Decin et al. 2011; Groenewegen et al. 2012); far ultraviolet (FUV) continuum (Sahai & Chronopoulos 2010); and spectral line emission from CO (e.g., Knapp et al. 1998; Fong et al. 2003; Cernicharo et al. 2014) and a host of other molecules (e.g., Olofsson et al. 1982; Cernicharo et al. 2000; Patel et al. 2009, 2011; De Beck et al. 2012). Such studies have established that the CSE of IRC+10216 is chemically complex and exhibits non-spherical structure on scales ranging from milliarcseconds (e.g., Tuthill et al. 2000; Weigelt et al. 2002; Leão et al. 2006) to tens of arcminutes (Sahai & Chronopoulos 2010; Ladjal et al. 2010). IRC+10216 has a moderately high space velocity (Table 1), and at large distances from the star (>0.3 pc), there are also visible signatures of interaction between the outermost CSE and the interstellar medium (ISM), including a bow shock ahead of the star, and a wide-angle "vortical tail" trailing its direction of space motion (Sahai & Chronopoulos 2010; Ladjal et al. 2010).

Despite the vast literature on the chemistry and morphology of the IRC+10216 CSE, comparatively little is known about the predominant component of the CSE by mass (∼70%)—the hydrogen gas. Outstanding questions include the total mass of the circumstellar hydrogen, the fraction that is in atomic versus molecular form as a function

of distance from the star, and the relationship (both spatial and kinematic) between the hydrogen gas and the dust and other molecules. Such information is important for deciphering the complex mass loss histories of stars like IRC+10216, including the amount of mass that they return to the ISM while on the AGB, and the details of their transition from AGB stars to planetary nebulae.

Glassgold & Huggins (1983; hereafter GH83) showed that for a given mass loss rate, the fraction of an AGB star wind that is comprised of molecular hydrogen versus atomic hydrogen is expected to depend largely on the stellar effective temperature, $T_{\rm eff}$, with the transition from predominantly atomic to predominantly molecular winds predicted to occur for $T_{\rm eff} \lesssim$2500 K. This is largely independent of whether the star has a carbon-rich or oxygen-rich atmosphere.

Effective temperature determinations for IRC+10216 are notoriously uncertain owing to the high opacity of the star's dusty envelope, and values in the literature show considerable scatter. However, with the exception of Men'shchikov et al. (2001), who proposed an effective temperature in the range 2500-3000 K based on a combination of radiative transfer and stellar evolutionary modelling, nearly all other published determinations lie within the temperature range where molecular hydrogen is expected to comprise the bulk of the wind and envelope: e.g., 2230 K (Cohen 1979); 1800 K (Phillips et al. 1982); 2330±350 K (Ridgway & Keady 1988); 2200±150 K (Ivezić & Elitzur 1996); 1915-2105 K (Bergeat et al. 2001).

Observations to date have supported the suggestion that the bulk of the IRC+10216 CSE is comprised of molecular rather than atomic gas (see §2 for details), and indeed, radiation from H_2 molecules has been proposed as the source of the extended FUV emission seen by *GALEX* (Sahai & Chronopoulos 2010). However, even for stars as cool as ∼2000 K, a thin shell of atomic hydrogen is predicted to form at the edge of the CSE as a result of photodissociation of H_2 and heavier molecules by the interstellar radiation field (Morris & Jura 1983; GH83). For slightly warmer stars ($T_{\rm eff}$ ∼2200 K), some small fraction of the hydrogen in the inner CSE ($\lesssim$1%) is also expected be atomic as a result of "freeze-out" of the photospheric abundances (GH83). In the case of IRC+10216, both processes are predicted to produce quantities of atomic hydrogen that are within the detection limits of modern radio telescopes (GH83). Furthermore, for stars like IRC+10216 that have appreciable space velocities, additional neutral hydrogen may be swept up from the ambient ISM (Villaver et al. 2002, 2012). Motivated by these predictions, we have undertaken a sensitive new search for atomic hydrogen in the IRC+10216 CSE using H I 21-cm line mapping observations obtained with the Robert C. Byrd Green Bank Telescope (GBT) of the National Radio Astronomy Observatory[1].

[1] The National Radio Astronomy Observatory is a facility of the National Science Foundation, operated under a cooperative agreement by Associated Universities, Inc.

Table 1. Coordinates and Stellar Properties of IRC+10216

Parameter	Value	Ref.
α (J2000.0)	09 47 57.4	1
δ (J2000.0)	+13 16 43.5	1
l	221.°45	1
b	+45.°06	1
Distance	130 pc	2
Spectral Type	C9,5e	3
Variability class	Mira	4
Pulsation period	639±4 days	5
$T_{\rm eff}$ [a]	∼2200 K	see §1
Photospheric diameter (optical)	3.8 AU	2
Luminosity	$8640\pm430 L_\odot$	2
Initial Mass	3-5 $M_\odot$	6
Current Mass	0.7-0.9 $M_\odot$	7
$\dot{M}$	2×10^{-5} $M_\odot$ yr^{-1}	8
$V_{\rm outflow}$	14.6±0.3 km s^{-1}	9
$V_{\rm LSR}$	-25.5 ± 0.3 km s^{-1}	9
Proper motion ($\mu_\alpha \cos\delta, \mu_\delta$)	(35±1,+12±1) mas yr^{-1}	2
$V_{\rm space}$	42 km s^{-1}	2
P.A. of space motion	70 degrees (E of N)	2

Units of right ascension are hours, minutes, and seconds, and units of declination are degrees, arcminutes, and arcseconds. All quantities have been scaled to the distance adopted in this paper.

[a] Based on a mean of various determinations in the literature.

(1) SIMBAD database; (2) Menten et al. 2012; (3) Cohen 1979; (4) Ridgway & Keady 1981; (5) Groenewegen et al. 2012; (6) Guelin et al. 1995; (7) Ladjal et al. 2010; (8) Crosas & Menten 1997; (9) Knapp et al. 1998

2 PREVIOUS H I 21-CM LINE OBSERVATIONS OF IRC+10216

Several previous authors have attempted to detect neutral atomic hydrogen associated with the CSE of IRC+10216. Here we briefly summarize these efforts to provide context for the current study. All stellar parameters quoted in this section have been scaled to the distance adopted in this paper.

Zuckerman et al. (1980) were the first to attempt detection of H I 21-cm line emission associated with mass loss from IRC+10216. Using the Arecibo telescope (which has a FWHM beamwidth at 21-cm of 3.′2), Zuckerman et al. obtained a position-switched (on−off) measurement with the "on" position centered on the star and the "off" measurement comprising an average of four pointings displaced by ±3.′5 in RA and ±3.′5 in DEC, respectively. No circumstellar H I emission was detected, and these authors placed a (1σ) upper limit on the H I mass within the Arecibo beam of $M_{\rm HI} < 6.3 \times 10^{-4}$ $M_\odot$.

Using observations obtained with the Very Large Array (VLA) in its C configuration, Bowers & Knapp (1987) also failed to detect any H I emission associated with IRC+10216. These authors placed a 3σ upper limit on the H I mass within a synthesized beam (50″ FWHM) centered on the stellar position of $M_{\rm HI} < 5.5 \times 10^{-5} M_\odot$ and a 3σ upper limit on the total CSE mass of $M_{\rm HI} < 1.0 \times 10^{-4}$ $M_\odot$ assuming a source diameter of 6′.

While these earlier results were somewhat discouraging, interest in detecting circumstellar hydrogen around evolved stars was reinvigorated roughly a decade later when Le Bertre & Gérard (2001) revisited IRC+10216 using the then newly upgraded Nançay Radio Telescope (NRT). The NRT has an elongated beam with a FWHM at 21 cm of ∼ 4′ east-west and ∼ 22′ north-south. Based on position-switched measurements where the "off" spectra comprised of the average of spectra displaced by ±4′, ±8′, and ±12′ in RA from

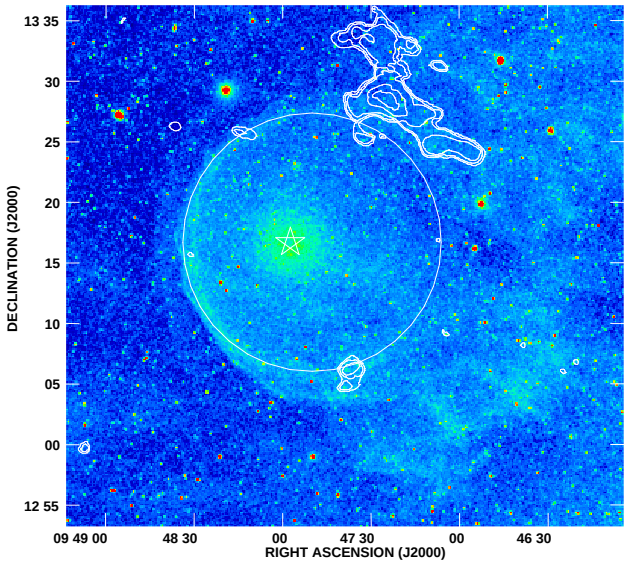

Figure 1. *GALEX* FUV image of IRC+10216 with VLA H I contours from MR07 overplotted. The contour levels are (6,12,18,38,48)×1.2 Jy beam^{-1} m s^{-1}. No correction for the VLA primary beam has been applied. The VLA synthesized beam was $\sim 101'' \times 94''$. A white star symbol indicates the stellar position. The overplotted circle has a diameter of $1280''$ and has been displaced by $110''$ west of the star (see §4.1 for details).

the stellar position, respectively, Le Bertre & Gérard found a surprising result: an H I *absorption* profile centered at the stellar systemic velocity, with a velocity width comparable to twice the outflow speed of the star. They attributed this finding to cold circumstellar in the outer CSE, seen in absorption against the cosmic microwave background radiation (but see below).

Motivated by the results of Le Bertre & Gérard (2001), Matthews & Reid (2007; hereafter MR07) obtained new H I imaging observations of IRC+10216 with the VLA, this time using its most compact (D) configuration to improve sensitivity to extended emission. Compared with the earlier observations of Bowers & Knapp (1987), the data of MR07 also had ∼2.5 times lower RMS noise (normalized to a $50''$ synthesized beam). Consistent with Bowers & Knapp, MR07 detected no H I emission directly toward the stellar position. However, MR07 did find several isolated clumps and arcs of emission displaced by ∼$11'$ to $18'$ (∼0.4 to 0.7 pc in projected distance) from the star. The velocities of these features are consistent with molecular gas previously observed at smaller radii in the CSE ($r \lesssim 120''$), leading MR07 to suggest that they could plausibly be circumstellar in origin. Assuming that the clumps and arcs detected with the VLA between LSR velocities −33 km s^{-1} and −17 km s^{-1} were associated with the CSE, MR07 derived a circumstellar H I mass of $\sim 2.2 \times 10^{-3}\ M_{\odot}$. The results of the VLA imaging also led MR07 to suggest an alternative interpretation for the apparent absorption spectrum seen by Le Bertre & Gérard (2001)—namely that the off-source spectra used for the position-switched NRT measurements may have been contaminated by H I *emission*, thus mimicking an absorption signature in on−off difference spectra.

A further twist came three years later, with the discovery of a FUV-emitting astrosphere surrounding IRC+10216 (Sahai & Chronopoulos 2010). Figure 1 shows a version of the FUV image with the VLA H I contours of MR07 overplotted. As pointed out by Matthews et al. (2011), this overlay is highly suggestive of a relationship between the H I clumps and arcs detected with the VLA and the circumstellar structures traced in FUV light by *GALEX*. However, the bulk of the H I emission detected with the VLA lies near, or just outside the ∼ $30'$ FWHM VLA primary beam, where sensitivity drops steeply, and a chance confusion with an interstellar cloud along the line-of-sight cannot be strictly excluded. At the same time, an interferometer like the VLA has rather poor sensitivity to diffuse, low surface brightness emission that is extended over scales of several arcminutes or more. This raises the possibility that there may be additional atomic hydrogen present in the IRC+10216 CSE that was not detected with the VLA, but which could be detectable through sensitive observations with a single-dish telescope.

For these reasons, we have embarked on a new investigation of IRC+10216 in the H I 21-cm line using the GBT. A combination of several attributes of the GBT make it particularly well-suited for such a study. Its 100-m aperture provides exceptional sensitivity, and its ∼ $9'$ FWHM beamwidth at 21 cm is comparable to the largest angular scales detectable in the VLA D configuration data of MR07. Furthermore, the extremely low sidelobe levels of the GBT main beam, coupled with the availability of new software to make robust stray radiation corrections (Boothroyd et al. 2011), insure that low-level extended emission can be reliably detected and characterized. Finally, unlike the NRT, which is a transit instrument, the GBT can perform on-the-fly mapping, allowing us to efficiently map the entire extended astrosphere and tail of IRC+10216 and also characterize the ISM across an extended region surrounding the star.

Shortly after our new GBT data were obtained, Menten et al. (2012) performed an investigation of the region around IRC+10216 using H I data from the Arecibo GALFA-H I survey (Peek et al. 2011a) and reported finding no sign of H I emission associated with the CSE. However, the GBT data have a surface brightness sensitivity ∼7 times higher than the GALFA-H I data, and as described below (§4), this improved sensitivity coupled with a more extensive analysis, has yielded some new information, including the detection of neutral hydrogen that appears to be associated with the IRC+10216 CSE.

3 OBSERVATIONS AND DATA REDUCTION

H I 21-cm spectral line mapping of a $2^{\circ} \times 2^{\circ}$ region surrounding IRC+10216 was obtained using the GBT during a series of seven observing sessions on 2011 November 16, 17, 20, 22, and 29 and 2011 December 6 and 7. Pointing and focus were checked at the start of each session using observations of a suitable continuum source. For the spectral line observations, the GBT spectrometer was employed with a 12.5 MHz bandwidth and 9-level sampling. In the raw data, there were 16,384 spectral channels with a 0.7629 kHz (0.16 km s^{-1}) channel spacing. In-band frequency switching was used with cycles of 0.8 Hz, alternating between frequency shifts of 0 and −2.5 MHz from the centre frequency of 1420.52 MHz

($V_{\rm LSR} = -25.5$ km s^{-1}). This resulted in a usable LSR velocity range from ~ -500 km s^{-1} to $+500$ km s^{-1}. Data were recorded in dual linear polarizations.

System temperatures over the course of our observing runs ranged from 11 K to 24 K, and mean values for each of the seven observing sessions ranged from 16.3 K to 18.6 K. Absolute calibration of the brightness temperature scale was determined from injection of a noise diode signal at a rate of 0.4 Hz and was checked for consistency during each session with observations of the line calibrator S6 (Williams 1973).

To maximize observing efficiency, we employed the on-the-fly (OTF) mapping technique (Mangum et al. 2007). Given the spatial extension of the IRC+10216 astrosphere and trailing wake previously seen in the FUV (Figure 1), we adopted a map centre 0.°25 west of the stellar position ($\alpha_{\rm J2000} = 09^{\rm h}47^{\rm m}00^{\rm s}$, $\delta_{\rm J2000} = 13^\circ16'43''.56$).

At the frequency of our observations, the FWHM of the GBT beam is $\theta \sim 8'.7$. We therefore used a spatial sampling of $1'.62$ (approximately two times higher than the Nyquist value of $\theta/2.4$) to avoid the beam degradation and decrease in the signal-to-noise ratio that occur with coarser sampling (see Magnum et al. 2007). We scanned in right ascension, and obtained several complete passes over the entire $2^\circ \times 2^\circ$ target region. Because observing time for our program was allocated dynamically, the size of the region mapped, the scan rate, and the dump time were adjusted from session to session to insure that we achieved a suitable balance between our two objectives: (1) obtaining a high sensitivity map across the IRC+10216 astrosphere; and (2) achieving sufficient spatial coverage to characterize the larger scale environment of the star. Scan rates ranged from 12 arcsec s^{-1} to 97 arcsec s^{-1} and dump rates between 1 and 4 seconds. A consequence is that our resulting map has a lower RMS noise level in the inner $1.^\circ0 \times 1.^\circ0$ compared with the outer $0.^\circ5$ border (see below). In total, 42.6 hours of data were used to construct our final map.

Initial data reduction steps were performed using GBTIDL[2]. The total power for each scan was computed using two reference spectra (during which the noise diode was fired) and two signal spectra. After combining these, the calibrated data were folded to average the two parts of the in-band frequency-switched spectrum. A handful of spectral channels that showed persistent radio frequency interference were flagged, and the data were then smoothed in frequency with a boxcar function (of kernel width 5) and decimated, resulting in spectra with a channel spacing of $\sim$0.8 km s^{-1}.

At this stage, the data were corrected for stray radiation using the approach developed by Boothroyd et al. (2011). These corrections are expected to reduce systematic errors in 21-cm line measurements with the GBT by as much as an order of magnitude, and are thus particularly important for studies like ours that aim to detect and characterize weak, extended emission,

Following the corrections for stray radiation, the data were imported back into GBTIDL. The flux density scale was converted from units of main beam brightness temperature to Janskys assuming a gain factor of 0.463 Jy K^{-1}, and a third order polynomial baseline was fitted and subtracted from each spectrum. The regions of the spectrum used for the baseline fits correspond to $-275 \lesssim V_{\rm LSR} \lesssim -120$ km s^{-1} and $133 \lesssim V_{\rm LSR} \lesssim 287$ km s^{-1}.

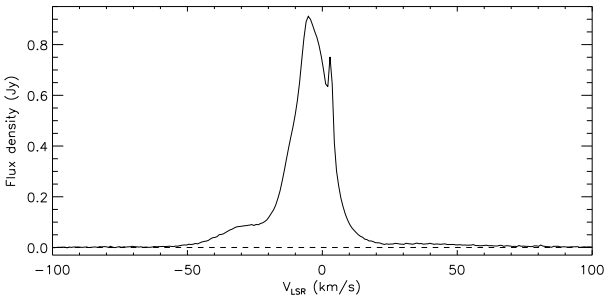

Figure 2. Frequency-switched GBT H I spectrum toward the position of IRC+10216. The emission was integrated over a 9-pixel ($300'' \times 300''$) region centered on the stellar position.

The baseline-subtracted spectra were converted to standard SDFITS format using the idlToSdfits program developed by G. Langston and subsequently imported into the Astronomical Imaging and Processing Software package (AIPS; Greisen 2003) for further processing and analysis. Within AIPS, the data from the seven different observing sessions were concatenated and then convolved and sampled onto a regular grid using the task SDGRD, resulting in a three-dimensional spectral line data cube. For the gridding, a Bessel∗Gaussian convolution function was used with cell size of $100''$. Other gridding parameters were optimized as per the recommendations of Mangum et al. (2007). The RMS noise in the resulting data cube is $\sim$5.5 mJy beam^{-1} per 0.8 km s^{-1} spectral channel within the central $1.^\circ0 \times 1.^\circ0$ of the maps and $\sim$20 mJy beam^{-1} along the outer $0.^\circ5$ border.

4 RESULTS

Despite the moderately high Galactic latitude of IRC+10216, H I line profiles toward its direction are complex and exhibit signatures of multiple interstellar emission components along the line-of-sight (Figure 2; see also Hartmann & Burton 1997). These interstellar emission components must be disentangled to allow identification of the much weaker circumstellar emission.

As an initial step toward characterizing the line-of-sight emission, we performed Gaussian decompositions of frequency-switched spectra near the position of IRC+10216. This analysis has yielded insights into the local interstellar environment of IRC+10216 as well as the other interstellar components toward this direction, including high- and intermediate-velocity gas and an emission component associated with the Local Leo Cold Cloud. Details are provided in Appendix. However, these spectral decompositions did not allow us to unambiguously identify any H I emission associated with the circumstellar environment of IRC+10216. For this purpose, it was necessary to take further advantage of the spatial information provided by our spectral mapping, including examination of H I channel maps and moment maps and constructing difference spectra using observations toward the CSE of IRC+10216 and at neighboring

[2] http://gbtidl.nrao.edu/

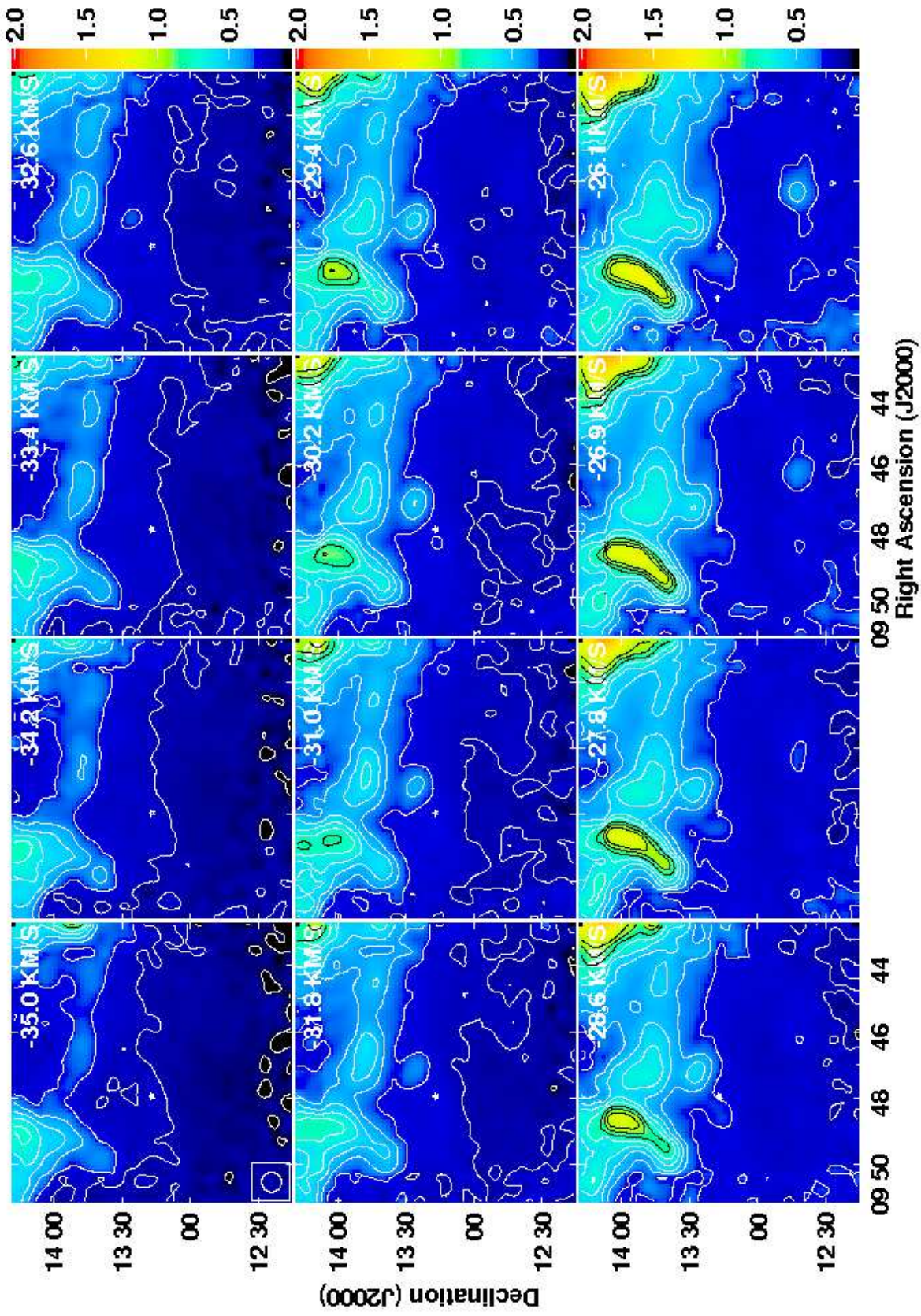

Figure 3. GBT H I channel maps at LSR velocities close to the stellar systemic velocity of IRC+10216 ($V_{\rm LSR,\star} = -25.5$ km s^{-1}.) Contour levels are (1,2,...10)×0.1 Jy beam^{-1}. The intensity scale has units of Jy beam^{-1}. A star symbol indicates the stellar position.

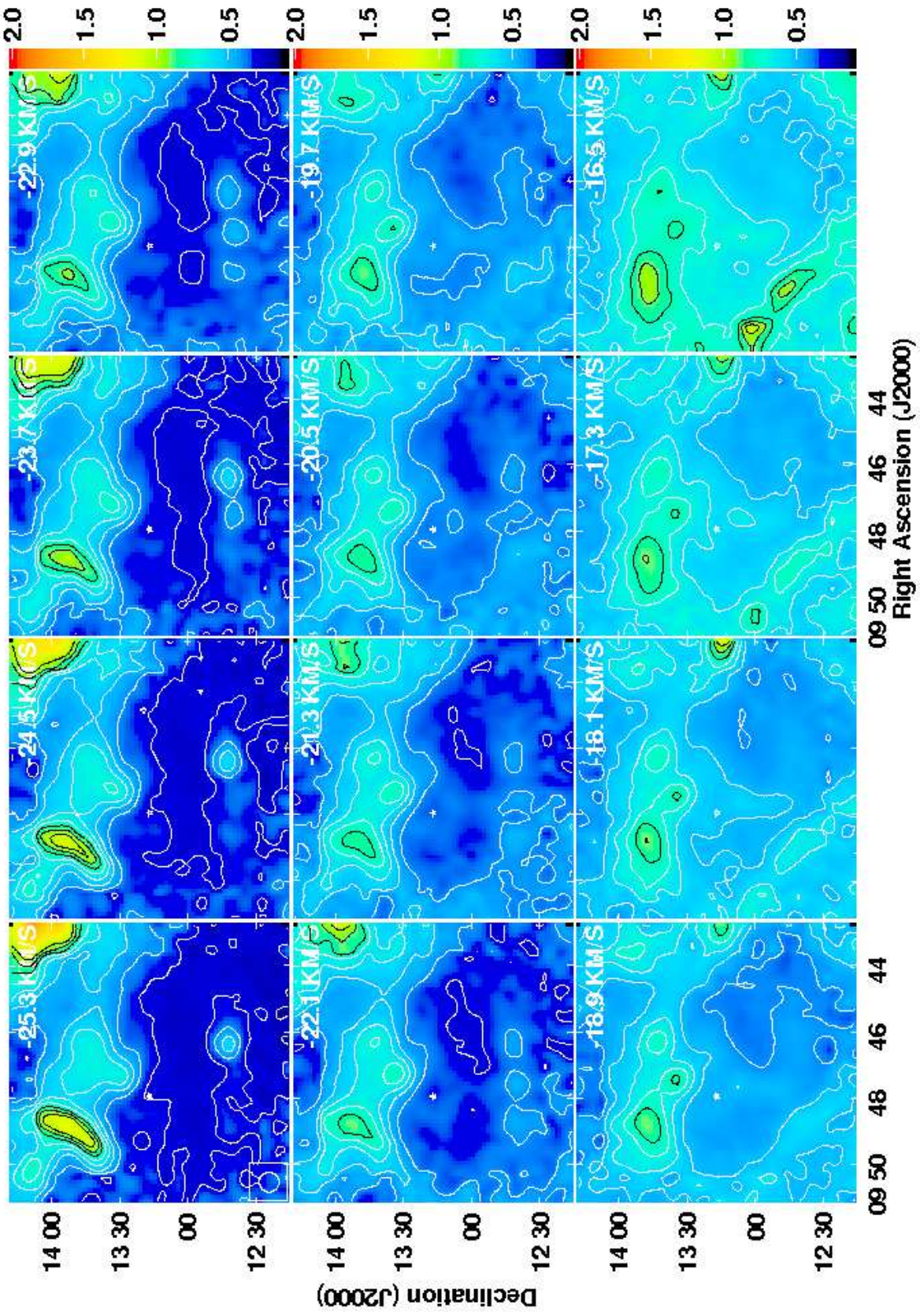

Figure 3 – *continued*

reference positions. The results of this analysis are described in the sections that follow.

4.1 Identification of H I Emission Associated with the IRC+10216 Astrosphere

Figure 3 presents a series of H I channel maps at velocities bracketing the systemic velocity of IRC+10216. We see that the bulk of the emission at these velocities lies in a spatially extended complex of clouds north of IRC+10216 that is almost certainly unrelated to mass loss from IRC+10216. Also present at these velocities is a set of three compact clouds south of IRC+10216 that appear to lie along a single linear filament near declination 12° 41′ and between right ascension $09^{\rm h}$ $46^{\rm m}$ and $09^{\rm h}$ $49^{\rm m}$. These clouds too are likely unrelated to the star.[3]

Although line-of-sight emission dominates the channel maps shown in Figure 3, inspection of the region near IRC+10216 reveals something interesting: evidence of a faint, shell-like structure surrounding the stellar position. A nearly complete shell is visible in several consecutive velocity channels redward of the stellar velocity, most notably in the channels centered at $V_{\rm LSR}$ = −22.1, −21.3, −20.5, and −19.7 km s^{-1}. The approximate diameter of the shell is $\sim 1280''$, or ∼0.8 pc at the distance of IRC+10216. An arc of emission consistent with the shell's location is also seen northeast of the star in velocity channels spanning $-30.2 \leqslant V_{\rm LSR} \leqslant -23.7$ km s^{-1}. Redward of $V_{\rm LSR} = -18.9$ km s^{-1}, background confusion begins to dominate and signatures of the shell are no longer readily apparent.

To further highlight the putative shell, in Figure 4 (top panel) we show an image produced by taking a mean of the emission over the velocity range $-24.5 \leqslant V_{\rm LSR} \leqslant -21.3$ km s^{-1}. In the bottom panel, we show on the same scale a *GALEX* FUV image of the region. Despite confusion with line-of-sight emission along the northern and western part of the shell, we see that it matches closely in both size and position with the FUV-emitting astropause surrounding IRC+10216. The geometrical centre of both the H I and FUV shells are also displaced by a comparable amount ($\sim 110''$) west of the stellar position (see also Figure 1). The implications of this are discussed in §5.

To estimate the mean, beam-averaged H I column density of the shell, we have computed a sum of channel images from $-24.5 \leqslant V_{\rm LSR} \leqslant -21.3$ km s^{-1} and integrated the resulting map over a semi-circular aperture with radius $r = 900''$, centered $110''$ west of the stellar position, and extending between position angles of +70° to +250°. The remaining position angles were excluded because of obvious contamination from a cloud complex north of the star. We find $N_{\rm HI} < 2.1 \times 10^{19}$ cm^{-2}. This value is formally an upper limit over the range of velocities used to construct our total intensity map because the shell is superposed on a pedestal of background emission. However, the total column density associated with the shell may be higher if additional circumstellar material is present at higher LSR velocities where it is obscured by line-of-sight confusion.

A region of enhanced surface brightness is visible along the northeastern edge of the shell in Figure 4, upstream of the star's direction of space motion (along a position angle of 70°; Table 1). The enhanced H I column density at this location is consistent with a build-up of atomic hydrogen near the bow shock region previously identified in FUV and FIR images (Sahai & Chronopoulos 2010; Ladjal et al. 2010). The observed region of enhanced H I column density also spans a similar range of position angles as the region where Sahai & Chronopoulos identified a sharp falloff in the FUV emission intensity, which they attributed to gas pile-up outside the astropause. Our new observations imply that not all of the gas in this vicinity is ionized, despite sufficiently high predicted gas temperatures. Assuming a strong shock approximation and that the bow shock is sweeping up a mostly atomic material from the surrounding ISM, then $T \sim \left(\frac{3}{16}\right) \mu m_{\rm H} V_{\rm space}^2 / k \approx 52,000$ K, where μ=1.3 is the mean molecular weight of an atomic gas comprising 90% H and 10% He, $m_{\rm H}$ is the mass of the H atom, k is the Boltzmann constant, and $V_{\rm space} \approx 42$ km s^{-1} is the space velocity of the star.

While the H I shell in Figure 4 is visible in channel images created from frequency-switched data, as noted above, it is superposed on a background of line-of-sight emission that is widespread in this region (see also §A4). To estimate the mass of the shell, we therefore have derived one-dimensional position-switched spectra by integrating over the entire shell in each individual channel map and differencing the result with neighboring reference spectra. For the on-source spectrum, we integrated the emission over the same semi-circular aperture as used for the column density determination described above. We then constructed the reference ("off") spectra by integrating in $600'' \times 1700''$ rectangular regions centered at positions offset $(+1200'', -100'')$ and $(-1500'', -100'')$ from the stellar position, respectively. These positions are offset one beamwidth east and west, respectively, from the outer boundaries of the H I shell, while the north-south extent of the reference apertures matches that of the semi-circular on-source aperture. To account for the small difference in integration area, a correction factor was applied to each reference spectrum before differencing with the on-source spectrum. The resulting spectra are shown in Figure 5.

From the spectrum in Figure 5 we computed the velocity-integrated H I flux density by taking the area underneath the resulting difference spectrum between LSR velocities of −29.4 km s^{-1} and −18.1 km s^{-1} (the velocity range over which emission at the location of the shell is visible in the individual channel maps). We find $\int S_{\rm HI} {\rm d}v \approx 0.40 \pm 0.04$ Jy km s^{-1}. The quoted error bar reflects the difference in the values obtained using the east and the west off-source spectra. To obtain an estimate of the total H I mass of the shell, we assume the shell is symmetric about the position angle of space motion (PA=70°) and multiple our measured value by a factor of two to account for the fact that the flux density was integrated over only half the shell. We also assume that no emission is present at higher LSR velocities where contamination be-

[3] These clouds appear qualitatively similar to the types of condensations expected in post-shock gas following the collision of a high-velocity gas cloud with the Galactic disc (Tenorio-Tagle et al. 1986). These features may therefore hold clues on the origin of the Local Leo Cold Cloud and the high- and intermediate-velocity gas components that all occur toward this region of the sky (see Stark et al. 1994 and the Appendix).

gins to dominate. These assumptions may lead to an uncertainty in our derived H I mass by as much as a factor of two. Thus our best estimate for the mass of the H I shell is $M_{\rm HI} \sim (3.2 \pm 1.6) \times 10^{-3}\ M_{\odot}$.

The H I shell seen in Figure 4a appears to have a central depression, and consistent with previous workers (§2), we find no compelling evidence of H I emission directly along the line-of-sight to IRC+10216. In Figure 6 we show difference spectra where the "on" spectrum was integrated over a single 100″ pixel centered on IRC+10216, and the reference spectra were extracted 1100″ east (just outside the H I shell) and 600″ east (along the H I shell) respectively. In the former case, there is no significant emission at the stellar systemic velocity, although there are hints of emission peaks on either side of $V_{\rm sys}$, within the velocity range expected for circumstellar gas (as indicated by the horizontal bar). Although this line profile is consistent with the type of "double-horned" profile expected for optically thin emission that fills the beam (e.g., Zuckerman 1987), we do not take this detection to be significant given that the blue wing of the line overlaps in velocity with the intermediate velocity gas that is widespread throughout the region (§A4), while the red edge of the profile ($V_{\rm LSR} \gtrsim -18$ km s^{-1}) is strongly contaminated by line-of-sight emission. Further, in the difference spectrum constructed with a reference position along the shell, the blue and red peaks disappear, and we see instead only an negative spectral feature whose velocity spread is consistent with the velocity extent of the shell at this position in the H I channel maps (Figure 3).

Integrating the first spectrum in Figure 6 across the velocity range of the CSE (but excluding velocities $V_{\rm LSR} \geqslant -18$ km s^{-1}) we derive an integrated H I flux density of $\sim$ 0.0078Jy km s^{-1}, translating to an H I mass of $M_{\rm HI} \leqslant 3 \times 10^{-5}\ M_{\odot}$. This is consistent with previous upper limits toward the stellar position reported by other authors (see §2). The simplest interpretation of these results is that the inner portions of the IRC+10216 are predominantly molecular, with at most a small atomic fraction. If we assume that the standard mass continuity equation holds for the inner wind region (e.g., Lamers & Cassinelli 1999) and adopt $r = 9.7 \times 10^{16}$ cm (50″), then $M_{\rm tot} \approx \frac{1}{3}\dot{M}r/V_{\rm out} = 0.014 M_{\odot}$ using the values of $\dot{M}$ and $V_{\rm out}$ from Table 1. Thus $M_{\rm HI}/M_{\rm tot} \leqslant$0.2%. According to GH83, an atomic wind fraction of this magnitude can be explained by photospheric freeze-out if the stellar effective temperature is ∼2200 K, whereas the atomic fraction should become negligible if $T_{\rm eff}$ ∼2000 K (see also §5).

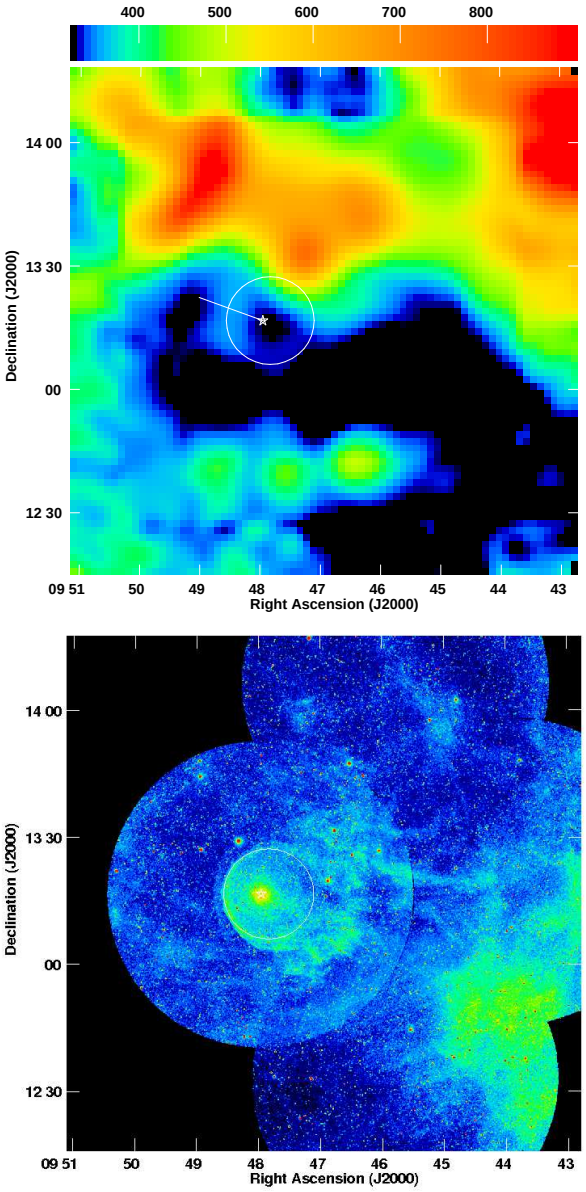

Figure 4. *Top:* H I intensity map obtained by averaging the emission over the velocity range $-24.5 \leqslant V_{\rm LSR} \leqslant -21.3$ km s^{-1}. The image is displayed using square root intensity scaling in units of mJy beam^{-1}. A star symbol denotes the position of IRC+10216, and the solid white line indicates its direction of space motion. *Bottom:* A *GALEX* FUV mosaic of the same field shown in the top panel. Identical circles with diameters of 1280″ are overlaid on both panels to highlight the location of shell-like structures visible at the respective wavelengths. The centres of the circles have been displaced by 110″ west of the stellar position.

4.2 H I Velocity Dispersion Map

In Figure 7 we present an H I velocity dispersion (second moment) map derived using data over the velocity range $V_{\star,\rm LSR} \pm 7.3$ km s^{-1}. This corresponds to the inner 50% of the range of gas velocities detected in molecular lines and is approximately the velocity range over which the H I shell is seen in our data. (Note however that this velocity range is larger than used to construct the H I intensity map in Figure 4a). Because of the imposed velocity cutoffs used to construct this velocity dispersion map, the absolute values of the gas dispersion are not physically meaningful. Nonetheless, this map offers a tool to disentangle emission related to the circumstellar environment of IRC+10216 from other line-of-sight emission. In particular, we find a coincidence between the peak velocity dispersion in the region ($\sigma_V = 4.5$ km s^{-1}) with the position of IRC+10216. This location has a small (∼0.2 km s^{-1}) but significant enhancement in velocity dispersion relative to the mean of its surroundings. Additional patches of slightly enhanced velocity dispersion are also seen both upstream and downstream of IRC+10216, along the trajectory of space motion of the star. It is unclear if these

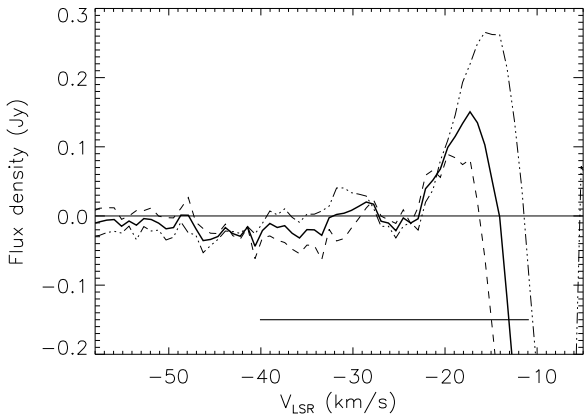

Figure 5. Position-switched spectrum of the H I shell. An on-source spectrum was constructed by integrating within a semi-circular aperture of radius 900″, centered on IRC+10216 and differenced with reference spectra extracted east of the star (dashed line) and west of the star (dot-dash line), respectively. See text for additional details. The thick line shows the difference spectrum obtained using a mean of the east and west reference positions. The horizontal bar indicates the expected range of gas velocities for the IRC+10216 CSE based on the outflow velocity measured from CO.

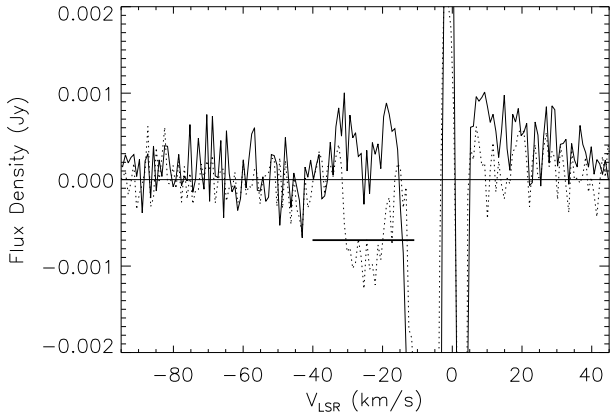

Figure 6. Position-switched spectra along the line-of-sight toward IRC+10216. An on-source spectrum was extracted over a singe 100″ pixel at the stellar position and differenced with reference spectra extracted 1100″ east (outside the H I shell; solid line) and 600″ east (along the H I shell; dotted line). In the latter spectrum, a negative feature is seen corresponding to the expected velocity range of the H I shell. The horizontal bar indicates the expected range of gas velocities for the IRC+10216 CSE based on the outflow velocity measured from CO.

are related to the motion of the star through the ISM, although in general, a region of enhanced turbulence may be expected within a foreshock zone lying just ahead of the bow shock (e.g., Blandford & Eichler 1987).

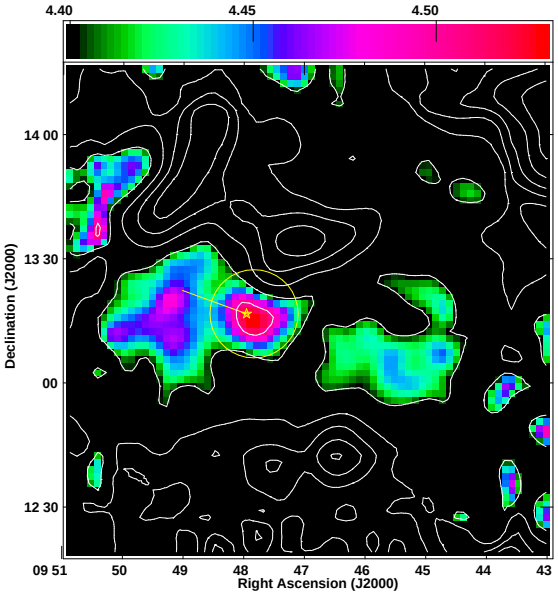

Figure 7. H I velocity dispersion map of the region around IRC+10216 (shown as both contours and color-scale), constructed by taking the intensity-weighted second moment of data spanning velocities $-32.5 \leqslant V_{\rm LSR} \leqslant -18.0$ km s^{-1}. The maximum velocity dispersion in the region is coincident with the location of the star. The overplotted circle is as in Figure 4, and the yellow line indicates the direction of space motion. Contour levels span 3.8 to 4.5 km s^{-1} in increments of 0.1 km s^{-1}. With the adopted intensity stretch, regions on the map with values $\leqslant 4.4$ km s^{-1} appear black. Because of the imposed velocity cutoffs used to construct the map, absolute values of the velocity dispersion are not physically meaningful.

4.3 Linking GBT and VLA Studies of the IRC+10216 Astrosphere

As previously noted, several of the small H I clumps previously detected with the VLA by MR07 align closely with the FUV-emitting astrosphere of IRC+10216 (Figure 1). These features are now also seen to overlap with the H I shell uncovered with the GBT (Figure 4). However, confirming an association between the VLA-detected "arcs" in the the northwest quadrant of Figure 1 and the CSE and/or vortical tail of IRC+10216 is less straightforward.

MR07 showed that the velocity distribution of the gas comprising the VLA arcs is consistent with a circumstellar origin. Matthews et al. (2011) also drew attention to what appears to be reflective symmetry between the H I arcs and morphologically similar FUV features in the southern part of the vortical tail. The authors speculated that the H I arcs might therefore represent a portion of the tail where the H I column density is enhanced because of preferential dissociation of molecular gas (e.g., due to an anisotropy in the UV radiation field).

As seen from a comparison of Figure 1 with the GBT channel maps in Figure 3, the VLA arcs lie near the southeastern rim of an H I cloud complex that extends across the northern portion of the channel maps at velocities close to the systemic velocity of IRC+10216 (see §A4). Within this cloud complex are regions of enhanced column density, including a compact "core" (unresolved by the GBT) lying in

the vicinity of the VLA arcs. Based on an H I total intensity map computed from GBT data spanning LSR velocities from -33 km s^{-1} to -17 km s^{-1} (the same range used to compute the VLA total intensity contours by MR07), the peak column density in the core is found to lie at $\alpha_{\rm J2000} = 09^{\rm h}47^{\rm m}20.3^{\rm s}$, $\delta_{\rm J2000} = 13^\circ32'31.9''$. This position is near the northernmost "lobe" of the VLA arc structures in Figure 1, but is $\sim$4.′3 northwest of where the peak column density in the arcs is measured.

The core seen with the GBT is embedded in a more extended envelope that extends southward to overlap with the position of the VLA arcs (and with the northern edge of the H I shell; see Figure 4); however, the column density varies smoothly across the location of the VLA arcs themselves. Thus it is possible that the VLA has filtered out much of the larger-scale emission along the line-of-sight to reveal discrete emission structures related to the IRC+10216 CSE and/or its wake that are obscured by confusion in the GBT map. That the curvature of the arcs follows the IRC+10216 astrosphere rather than the edge of the cloud seen in the GBT map is also consistent with this possibility. On the other hand, the gas velocities associated with the arcs are predominantly blueshifted relative to the stellar systemic velocity, in contrast to what is expected for material in a trailing wake or a circumstellar shell, where drag from the ISM tends to shift velocities toward zero LSR velocity. We conclude that an association between the VLA arcs and the astrosphere of IRC+10216 remains plausible, although we cannot unambiguously rule out line-of-sight confusion and are unable to explicitly identify a counterpart to the arcs in the GBT data.

4.4 Is There H I Emission Associated with the "Vortical Tail"?

We have searched our GBT data for H I emission at other locations within the FUV-defined vortical tail of IRC+10216, outside of where H I emission features were detected with the VLA. Figure 8 shows a position-switched spectrum, constructed by integrating over a $310'' \times 450''$ box, centered at $\alpha_{\rm J2000} = 09^{\rm h}46^{\rm m}2.2^{\rm s}$, $\delta_{\rm J2000} = 13^\circ19'33.0''$, and differencing with a comparable "off" spectrum offset $500''$ to the west. Gradients in the line-of-sight emission between these two locations result in a residual slope across the velocities of interest in the resulting difference spectrum, but we see no compelling evidence for a distinct component of H I emission associated with the tail. Based on this spectrum, we place a 3σ upper limit on the H I mass in the tail over the velocity range $-40 \leqslant V_{\rm LSR} \leqslant -18$ km s^{-1} of $M_{\rm HI} < 9.8 \times 10^{-3}\ M_\odot$.

The lack of an H I counterpart to the vortical tail seems somewhat surprising given that the tail lies exterior to the H I shell and therefore should be susceptible to molecular dissociation by the interstellar radiation field. One possibility is that gas in the tail has been decelerated as a result of its interaction with the ISM (see Matthews et al. 2008, 2011) and thus would emit at velocities shifted further toward zero LSR velocity compared with gas in the shell. In this case, H I emission redward of $V_{\rm LSR} \gtrsim -18$ km s^{-1} and near the location of the vortical tail would become impossible to disentangle from the background emission in our present data. Another possibility is that at least some of the FUV emission that appears associated with the tail instead lies in the foreground or background and is unrelated to the star.

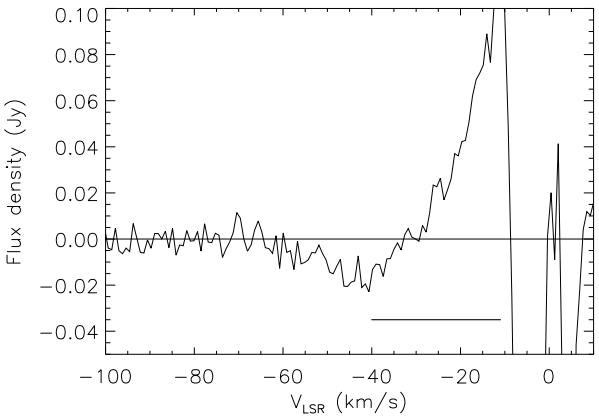

Figure 8. Position-switched spectrum obtained by differencing a spectrum integrated over the southern portion of the FUV-emitting vortical tail of IRC+10216 with a reference spectrum centered at a position $500''$ to the west. See §4.4 for details. Across the velocity range expected for the IRC+10216 CSE (indicated by the horizontal bar) the line-of-sight emission exhibits a steep gradient with position, but there is no unambiguous evidence of emission associated with the IRC+10216 tail. Strong line-of-sight confusion at velocities $V_{\rm LSR} \gtrsim -18$ km s^{-1} precludes identification of a possible counterpart to the tail at higher velocities.

Our GBT data provide insight into another question concerning the wake of debris trailing IRC+10216. An inspection of the *GALEX* image shown in Figure 4 reveals what appears to be a filament connecting the vortical tail of IRC+10216 to a spatially extended complex of FUV emission to the southwest of the star. Because this emission lies downstream from the direction of IRC+10216's space motion (see Table 1), this raises the intriguing possibility that the FUV-emitting material might correspond to debris from a previous mass-loss phase of IRC+10216. However, as we show in §A2, the complex of FUV emission to the southwest is correlated with enhanced H I emission at a velocity of $V_{\rm LSR} \approx +3.5$ km s^{-1} that can be attributed to the Local Leo Cold Cloud and therefore appears to be unrelated to IRC+10216.

5 DISCUSSION

We have reported the discovery of a low surface brightness H I shell associated with the astrosphere of IRC+10216. Several lines of evidence support an association between the H I shell and the IRC+10216 astrosphere rather than a chance superposition of emission along the line-of-sight: (1) the H I shell matches closely in both size and position with the FUV-emitting shell previously detected with *GALEX* (see Figure 4); (2) the central star is offset by $\sim 110''$ relative to the centre of the H I shell, in the direction expected for a star moving through the ISM (see below); (3) the narrow H I linewidth of the shell relative to the wind outflow speed (8.1 km s^{-1} compared to 14.6 km s^{-1}) and the small offset in velocity of the peak shell emission toward zero LSR velocity compared with the stellar systemic velocity (-23.8 km s^{-1}

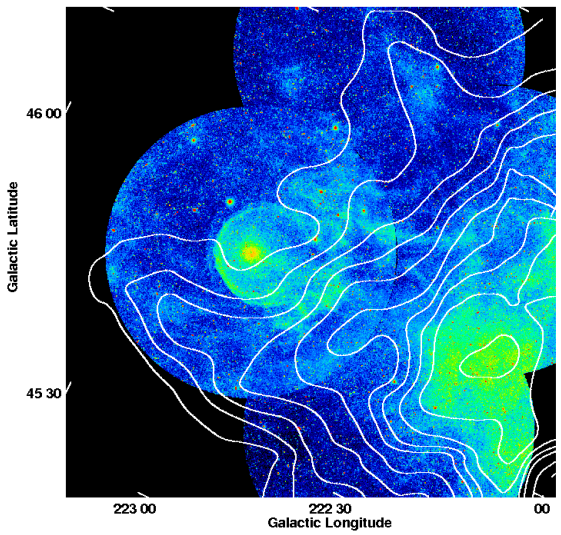

Figure 9. *GALEX* FUV image of IRC+10216 with GBT H I contours at $V_{\rm LSR}$ = 3.5 km s^{-1} overplotted. H I emission at this velocity is dominated by the LLCC (see §A2). Contour levels are (1,2,3...7.5,8,8.5,9.5,10)×1.2 Jy beam^{-1}. A region of enhanced FUV surface brightness southwest of IRC+10216 coincides with the highest H I column density at this velocity, implying that this material is linked with the LLCC and is not debris shed by IRC+10216. A Galactic coordinate system is used to illustrate the orientation of the LLCC contours relative to lines of constant Galactic latitude.

versus −25.5 km s^{-1}) are both consistent with H I shells detected around other stars, and can be explained by the interaction between the shell and the surrounding ISM (Gérard et al. 2011; Le Bertre et al. 2012; Matthews et al. 2013); (4) we observe an enhancement in the H I column density along the leading edge of the shell, where gas pile-up is expected (Figure 4); (5) we detect a region of enhanced velocity dispersion coincident with the location of the IRC+10216 CSE (§4.2). In the sections that follow, we comment on the possible origin of the detected H I shell and place constraints on its age and on the fraction of the total CSE mass that is comprised of H I gas.

5.1 The Origin of the Atomic Hydrogen in the Circumstellar Environment of IRC+10216

Our new observations are consistent with past indications that the bulk of the hydrogen gas in the circumstellar environment of IRC+10216 is in molecular form. Nonetheless, while the fraction of atomic hydrogen in the CSE is small, understanding the origin of this material provides important insights into the atmospheric physics of IRC+10216, as well as on the interaction between this mass-losing star and its interstellar environment.

If the effective temperature of IRC+10216 is sufficiently warm ($T_{\rm eff}$ ∼2200-2300 K), then model atmospheres predict that some small fraction of its wind ($\lesssim$1%) may be in atomic form within a few stellar radii owing to freeze-out—i.e., the cessation at some critical density and pressure of the three-body recombination needed to create H_2 (GH83). As described in §4.1, our upper limit on the mass of H I directly along the line-of-sight to IRC+10216 is consistent with a photospheric freeze-out abundance of H I of $\lesssim$0.2%. However, while even such a small fraction of atomic material in the wind may produce an observable signal when integrated over a sufficient volume, the observed radial distribution of H I column density for the case of a steady, spherically symmetric wind scales as the inverse of the projected distance from the star, resulting in a centrally peaked distribution (e.g., Bowers & Knapp 1988). This is in contrast to the shell with a central hole that we observe surrounding IRC+10216. This implies that some other mechanism to produce H I is needed to fully explain the current observations.

We note that the low observed H I fraction of the IRC+10216 wind appears to be inconsistent with the stellar effective temperature of 2500-3000 K advocated by Men'shchikov et al. (2001). Such a high value for the stellar effective temperature would imply that hydrogen is mostly in atomic form in the star's atmosphere (GH83). As the H/H_2 abundance ratio should be frozen out in the expanding wind, we therefore should have easily detected the H I line with an intensity $\geqslant$100 larger than observed. This argument is supported by the detection of the H I line in a number of stars with effective temperatures larger than 2500 K (Gérard & Le Bertre 2006, Matthews et al. 2013). The latter detections also suggest that atomic hydrogen does not in general recombine efficiently into molecular hydrogen within the outflows of these warmer stars.

One plausible candidate for the origin of the H I surrounding IRC+10216 is dissociation of H_2 molecules by the interstellar radiation field. Adopting estimates for the expected strength of the interstellar radiation field and the efficiency of the absorption of UV photons in the Lyman and Werner bands of H_2, Morris & Jura (1983) provided a simple analytic formula to predict the total number of hydrogen atoms in a circumstellar shell expected to arise from photodissociation: $n_{\rm H} \approx 1.8 \times 10^6 r^3/V_{\rm out}$. Taking r =0.4 pc and converting the result to solar mass units, we find $M_{\rm HI} \sim 1.9 \times 10^{-3}\ M_\odot$, in agreement, to within uncertainties, with our measurement (§4.1). The radial column density profile in this case should also peak in the outskirts of the CSE, consistent with our data.

Of course these agreements with the predictions from Morris & Jura (1983) must be treated cautiously since their formula relies on a number of simplifying assumptions. These include a particular (isotropic) strength for the Galactic radiation field and a constant, isotropic mass-loss rate for the entire age of the CSE. However, the interstellar radiation field unlikely to be uniform for a star well out of the Galactic plane, while the assumption of constant, isotropic mass loss is also questionable for IRC+10216, given the complex shells and other structures seen in the inner portions of the CSE at various wavelengths, suggesting that the recent mass-loss rate has been variable and punctuated by discrete episodes of enhanced mass loss. Further, some of the mass loss events may have have been non-isotropic (see references given in §1). Nonetheless, in principle, it may be realistic to assume that the total mass lost during these discrete events may be small compared with the mean mass-loss rate over the past ∼ 10^5 yr (e.g., Figure 8 of Vassiliadis & Wood 1993; see also §5.2).

One other key factor that needs to be considered is that the model of Morris & Jura (1983) assumes that the stellar wind is in free expansion throughout the CSE and does not

take into account the motion of the star through the ISM. In general, such motion can dramatically affect the shape, structure, density, and kinematics of the CSE, as well as its chemistry. For example, the motion is expected to introduce axisymmetries in the CSE, and the star is expected to become offset from the CSE centre (Villaver et al. 2012). Size segregation of dust grains may also result (van Marle et al. 2011).

IRC+10216 is known to be moving through the ISM with a moderately high space velocity (Table 1), and the bow shock and vortical tail structures seen in FIR and FUV images are clear manifestations of this interaction. Interaction with the ISM may also account for the observation that the H I shell detected with the GBT is primarily seen at LSR velocities higher than the systemic velocity. This type of velocity offset toward $V_{\rm LSR}$=0 km s^{-1} is a well-established hallmark of ISM interaction and has now been seen in a number of other H I-detected AGB stars (Gérard et al. 2011). Finally, the ISM interaction naturally explains the offset (by $\sim 110''$) of the star relative to the centre of the H I shell (see Figure 4).

Another prediction of hydrodynamical models is that the interaction with the ISM may lead to significant quantities of interstellar hydrogen being swept into the circumstellar environment (Villaver et al. 2002, 2012). This, for example, may account for the arc of H I emission we detect along the leading edge of the shell, near the bow shock region, and which exhibits a larger spread of gas velocities compared with the other portions of the shell (see Figure 3 and §4.1). An analogous phenomenon is seen in the case of solar-like stars moving through the ISM, leading to the formation of a so-called "hydrogen wall", just interior to the bow shock (Wood et al. 1996). In the case of IRC+10216, to account for the observed mass of H I within a volume of radius r=0.4 pc purely from swept-up interstellar material would require an ambient H I density of $n_{\rm HI} \sim 0.078$ atoms cm^{-3}, a value that is quite plausible even for a star well out of the Galactic Plane. Further, if we assume in the strong shock approximation that the velocity of the interstellar gas is reduced by a factor of 4 when it crosses the bow shock, ISM gas streaming at 42 km s^{-1} in the rest frame of the star would be reduced to a velocity of ∼10 km s^{-1}, or 6 km s^{-1} when projected along the line-of-sight. Thus the predicted LSR gas velocities in the shell might be expected to lie roughly in the range between −19 to −25 km s^{-1}, consistent with what we observe.

One additional possibility for producing atomic hydrogen in the IRC+10216 CSE may be related to the same emission mechanism responsible for the FUV emission from the astrosphere. The projected overlap between the H I shell that we have detected with the GBT and the FUV-emitting shell detected by *GALEX* suggests that the gas giving rise to the two structures could be co-spatial. Sahai & Chronopoulos (2010) proposed that the FUV luminosity of IRC+10216 is likely to be due to collisional excitation of H_2 molecules by hot (∼30 eV) electrons, analogous to the mechanism that Martin et al. (2007) proposed to explain the FUV-emitting wake of Mira. In this model, the dissociation of H_2 molecules is expected to be a byproduct of the excitation process (Raymond et al. 1997) and should result in the steady production of hydrogen atoms. Assuming a dissociation rate of $\sim 10^{42}$ s^{-1} (a third the rate assumed for Mira; see Martin et al.) implies that the entire observed mass of H I in the IRC+10216 could be produced in ∼60,000 yr. This assumes that the formation of new molecules would not occur efficiently in the outer CSE because of the low gas densities, the absence of dust grains at these radii (Decin et al. 2011), and the decreased shielding from the interstellar radiation field. However, this mechanism for producing H I also assumes that there will be a source for the hot electrons in the astrosphere. The stellar space velocity assumed by Sahai & Chronopoulos (91 km s^{-1}) is higher than the recent determination by Menten et al. (2012), and consequently, the temperature that we estimate for post-shock gas in the bow shock region (≈52,000 K; see §4.1) seems too low to produce the ∼30 eV electrons required.

5.2 Age Dating the CSE

One of the hydrodynamical models presented by Villaver et al. (2012) represents a star quite similar to IRC+10216, having initial mass of $3.5M_\odot$ and moving with a space velocity of 50 km s^{-1} through an interstellar medium with a particle density of 0.1 cm^{-3}. Examining Figure 12 of Villaver et al. at a time $t \sim (3.3-3.6)\times10^5$ yr since the start of the AGB, we note rather good agreement between the predicted size of the CSE and what is observed for IRC+10216. Further, the Villaver et al. model predicts that a nearly spherical shell of enhanced hydrogen density should circumscribe the entire CSE, consistent with our GBT results and with the FUV structures seen by *GALEX* east of the star.

The age of the IRC+10216 astrosphere implied by the comparison with the Villaver et al. model predictions is roughly an order of magnitude larger than the age of the shell computed from its dynamical crossing time (∼27,000 yr, assuming r ≈0.4 pc and $V_{\rm outflow}$=14.6 km s^{-1}) and roughly five times larger than the value of ∼69,000 years derived by Sahai & Chronopoulos (2010) based on assumptions about the expansion timescales for the shocked and unshocked wind regions. This underscores the importance of taking into account the effects of interaction with the surrounding ISM when age-dating circumstellar ejecta (see also Matthews et al. 2008, 2011).

5.3 Comparison of the Predicted Versus the Observed CSE Mass

Assuming the age of the IRC+10216 CSE to be $t \sim 3.5 \times 10^5$ yr (see §5.2), we can readily infer that the mass of atomic hydrogen that we observe to be associated with IRC+10216 ($M_{\rm HI} \sim 3\times10^{-3}\ M_\odot$) is only a tiny fraction of the expected total mass of the CSE. For example, assuming that IRC+10216 has been losing mass at its current high rate for ∼60,000 yr and at a lower rate prior to this (see Figure 2 of Villaver et al. 2012), the CSE mass should be $\gtrsim 1.2\ M_\odot$.

FIR observations also point to a significantly larger CSE mass than we have measured from H I. Based on 100μm observations from *Herschel*, Decin et al. (2011) estimated a mass for the IRC+10216 CSE within a radius $r < 390''$ of $\sim 0.17M_\odot$ (scaled to our adopted distance), assuming a gas-to-dust ratio of 250 (which is likely lower than the true value, making the discrepancy even more severe; see, e.g., Groenewegen et al. 1998). Our observations therefore support

earlier assertions, both theoretical and observational, that most of the mass loss from IRC+10216 has been in molecular form (e.g., Zuckerman et al. 1980; Bowers & Knapp 1987) and that dust and molecular self-shielding are able to preserve a large fraction of molecular gas even at large distances from the star $r > 10^{17}$ cm (Morris & Jura 1983; GH83).

For completeness, we note that there is another type of effect that in principle may lead to an underestimate of the amount of H I measured in very cool CSEs, namely self-absorption and/or absorption of the background emission (e.g., Levinson & Brown 1980). Based on Reich & Reich (1986), the background temperature of the continuum near IRC+10216 is ∼3.4 K, while from Figure 2, the H I background over the velocity range of the circumstellar shell is ∼0.1 Jy (0.2 K). Thus the total background is ⩽3.6 K, and for absorption to be occurring in the shell gas, its temperature must be lower than this. While such low temperatures have been reported in the circumstellar environments of some AGB and post-AGB sources (Sahai 1990; Sahai & Nyman 1997), they are expected to be achieved only in a freely expanding wind region where cooling is efficient, not within the zone where circumstellar matter is slowed by the ISM (e.g., Villaver et al. 2002), nor in the region inside the bow shock, where the pile-up of interstellar matter may occur. Absorption effects are thus likely to affect our H I mass estimate for IRC+10216 only directly along the line-of-sight to the star (where the telescope beam samples gas close to the star that is still in free expansion) and only if the atomic gas fraction in the wind as it leaves the star is larger than predicted by current models for stars with $T_{\rm eff} \lesssim 2500$ K (see §1). However, in this case, the line profile shape would be expected to be rectangular or parabolic, depending on its extent relative to the telescope beam (Zuckerman 1987), in contrast to what is observed toward the stellar position (Figure 6).

6 SUMMARY

Using sensitive H I mapping observations obtained with the GBT, we have uncovered evidence for an H I shell of radius ∼0.4 pc and a total H I mass $\sim (3.2 \pm 1.6) \times 10^{-3} M_{\odot}$ surrounding the carbon star IRC+10216. The H I shell is comparable in position and scale to the star's previously discovered FUV-emitting astrosphere (Sahai & Chronopoulos 2010) and encompasses some of the H I emission clumps previously seen encircling the star in H I maps obtained with the VLA by MR07. An enhancement in H I column density is seen along the leading edge of the H I shell (near the previously identified bow shock region), indicating a pile-up of neutral gas at this location. We find no evidence for atomic hydrogen associated with the wide-angle, FUV-emitting vortical tail that trails the motion of the star through the ISM, although line-of-sight confusion could have precluded detection if gas in the tail has been significantly decelerated as a result of interaction with the ISM.

The quantity of atomic hydrogen that we observe in the circumstellar environment of IRC+10216 is less than 1% of the total predicted mass of the CSE and is comparable to quantities of atomic hydrogen expected to originate from photodissociation of a predominantly molecular wind or from matter swept from the surrounding interstellar medium. Assuming that the FUV emission from the astrosphere arises from collisional excitation of H_2 molecules by hot electrons, the resulting collisional dissociation of molecules may also contribute to the observed H I mass. Finally, a small fraction of the observed atomic hydrogen may result from freeze-out in the photosphere, but the observed radial column density distribution of H I is inconsistent with this being the sole origin of the gas.

The H I shell that we detect surrounding IRC+10216 may be a precursor of the large atomic gas shells reported previously around some planetary nebulae (Taylor et al. 1989; Rodríguez et al. 2002) and that are predicted by hydrodynamic models to occur during the evolution of mass-losing AGB stars moving through the ISM (Villaver et al. 2002, 2012). The detection of H I associated with the CSE of IRC+10216 demonstrates the feasibility of mapping the kinematics of the CSEs of other evolved stars with low stellar effective temperature ($T_{\rm eff} \lesssim 2500$ K) despite the fact that their winds may be predominantly molecular.

ACKNOWLEDGMENTS

LDM would like to thank J. Lockman and other members of the NRAO Green Bank staff for guidance in the acquisition and reduction of the GBT data presented here and E. Greisen for new developments in AIPS that aided in the analysis of these data. These observations were taken as part of NRAO program AGBT11B_013. LDM also gratefully acknowledges financial support from grant AST-1310930 from the National Science Foundation.

APPENDIX A: CHARACTERIZING THE ISM IN THE DIRECTION OF IRC+10216

Frequency-switched H I spectra toward the direction of IRC+10216 are complex, comprising a blend of multiple velocity components (e.g., Hartmann & Burton 1997). The characterization of these components is important for identifying and interpreting circumstellar emission and also provides insight into the local interstellar environment of the star. In this Appendix, we provide a brief description of the main spectral components present along the line-of-sight to IRC+10216 based on the analysis of our new GBT data, coupled with information from previously published studies.

Figure 2 (already discussed in §4) shows a frequency-switched H I spectrum toward the direction of IRC+10216. Using the AIPS task XGAUS (Greisen 2014), we have performed a Gaussian decomposition of the line profile and find that a minimum of six emission components is required to adequately reproduce the spectrum. The results of the best-fitting decomposition (as determined by χ^2 minimization) are summarized in Table A1.

Given the large number of components in the fit, the decomposition presented in Table A1 may not be unique. We also ignore the possibility of absorption components and/or optical depth effects that might result in non-Gaussian emission profiles (see Verschuur & Knapp 1971; Haud & Kalberla

Table A1. Gaussian Decomposition of H I Spectrum toward IRC+10216

Component	Amplitude (mJy)	$V_{\rm LSR}$ (km s^{-1})	FWHM (km s^{-1})
1	72±1	-29.0 ± 0.2	19.5±0.5
2	160±8	-5.82 ± 0.04	3.7±0.1
3	668±8	-4.66 ± 0.05	16.5±0.1
4	185±8	−1.0±0.1	7.6±0.4
5	292±4	+3.17±0.01	1.66±0.03
6	19±1	+7.9±1.6	92.0±2.8

Fit components and their uncertainties were determined using the AIPS task XGAUS. The fitted spectrum was integrated over a $300'' \times 300''$ region centered on the position of IRC+10216. The RMS residual was 2.6 mJy over the fitted LSR velocity range from −75 to 87 km s^{-1}.

2006). However, despite these caveats, we find these fit results are instructive for guiding the discussion that follows.

A1 ISM Local to IRC+10216?

In terms of peak column density, the dominant spectral component in Figure 2 is centered near $V_{\rm LSR} \approx -4.7$ km s^{-1} (viz. Component 3 in Table A1). Two other weaker components (2 and 4 in Table A1) are also found at similar velocities (−5.8 km s^{-1} and −1.0 km s^{-1}, respectively). Toward the Galactic latitude and longitude of IRC+10216, all three of these components have velocities consistent with values expected for gas in regular Galactic rotation (Hartmann & Burton 1997). This implies that some of this gas may be local to the star or lie within its Galactic neighborhood. However, this remains unconfirmed, and to our knowledge, no interstellar absorption features have been unambiguously detected at comparable velocities in the spectra of background stars in this region (Kendall et al. 2002; Mauron & Huggins 2010).

A2 The Local Leo Cold Cloud (LLCC)

A second dominant component in our GBT spectrum (Component 5 in Table A1) is centered near $V_{\rm LSR} \approx +3$ km s^{-1} and has a rather narrow linewidth (FWHM≈1.7 km s^{-1}), indicating the presence of very cold gas. We attribute this component to the well-known Local Leo Cold Cloud (LLCC). Portions of the LLCC were first discovered by Verschuur (1969), and Haud (2010) later showed that the emission detected by Verschuur is actually part of a vast ribbon of clouds of similar linewidths and velocities, stretching from approximately 7 hr to 11 hr in RA and −10° to +40° in DEC. Using stellar absorption line measurements, Peek et al. (2011b) constrained the distance of the LLCC to lie in the range 11.3 pc to 24.3 pc—i.e., in the foreground of IRC+10216 and comfortably inside the Local Bubble. Peek et al. also demonstrated a clear correlation between the H I emission from the LLCC and 100μm dust emission.

Within the region we have mapped with the GBT, we find that the highest LLCC H I column densities correlate with a region of enhanced FUV surface brightness to the southwest of the IRC+10216 astrosphere (Figure 9). This correlation implies that this FUV-emitting material is not debris shed by IRC+10216, despite its location downstream of IRC+10216's space trajectory and in spite of what appear to be FUV-emitting filaments connecting this cloud to the astrosphere.

A3 High-Velocity Halo Gas?

Broad, high-velocity wings are another feature of the spectrum shown in Figure 2. These wings are also seen in the GALFA spectrum presented by Menten et al. (2012), confirming they are not artefacts caused by poor baseline fits or erroneous stray radiation corrections. At positive LSR velocities, low-level emission can be seen stretching to velocities as high as ∼100 km s^{-1}, and we were able to parametrize this with a broad Gaussian of FWHM∼91.5 km s^{-1}, centered at $V_{\rm LSR} = 7.9$ km s^{-1} (Component 6 in Table A1). While it is reasonable to question whether the large gas dispersion implied by such a broad Gaussian is physically meaningful, we note that similarly broad Gaussian components have been reported by other workers at high Galactic latitude and have been suggested to arise from halo gas with a high velocity dispersion (Kalberla et al. 1998; Haud & Kalberla 2006).

Regardless of whether the extended red line wing in the spectrum represents a single velocity component or a blend of several along the line-of-sight, the presence of gas extending to such high velocities cannot be accounted for by Galactic disc rotation, particularly given the relatively high Galactic latitude of IRC+10216 (Stark et al. 1994; Hartmann & Burton 1997). Indeed, based on maps presented by Wakker & van Woerden (2013), the IRC+10216 field lies near the outskirts of the "WA" high-velocity cloud complex, which is characterized by LSR velocities in the range 80-195 km s^{-1} (Wakker & van Woerden 1991). An association between the high positive velocity gas we observe and the WA complex is therefore possible. Distance estimates to the WA complex place this material at 15-20 kpc (Wakker & van Woerden 2013), or well out in the Galactic halo.

A4 Blueshifted Intermediate Velocity Gas

At negative LSR velocities, a "shoulder" of emission is seen blueward of $V_{\rm LSR} \lesssim -20$ km s^{-1} in the spectrum in Figure 2. In the fit presented in Table A1, we have characterized this emission with a Gaussian centered at $V_{\rm LSR} \approx -29$ km s^{-1} and a FWHM linewidth of 19.5 km s^{-1} (Component 1 in Table A1). The peak column density of this component therefore occurs at a velocity close to the stellar systemic velocity of IRC+10216, and indeed, as described in §4.1, there is evidence that a small portion of this emission is in fact related to the IRC+10216 CSE. However, as seen from our own channel maps of the region (Figure 3), as well from larger-scale maps of Galactic H I (e.g., Hartmann & Burton 1997), gas spanning these velocities is widespread throughout the region, particularly to the north of IRC+10216, and is far too pervasive to be accounted for entirely from mass loss from IRC+10216.

In optical absorption line spectra of three stars within 2.°5 of IRC+10216, Kendall et al. (2002) detected an absorption feature at $V_{\rm LSR} \approx -10$ km s^{-1} that they attributed to a diffuse interstellar band. One of the targets stars lies in the foreground of IRC+10216 (at a distance of ∼55 pc), and Menten et al. (2012) argued that gas at even higher negative velocities is also likely to lie in the foreground of IRC+10216. While this cannot be excluded, Menten et al.'s arguments are based on the assumption of monotonic Galactic rotation. However, we note that toward the direction of IRC+10216, gas velocities of $|V_{\rm LSR}| \gtrsim 20$ km s^{-1} are "forbid-

den" and lie outside the range nominally expected for disc rotation (e.g., Hartmann & Burton 1997). Thus according to the definition of Wakker & van Woerden (2013), the material comprising Component 1 in our spectrum qualifies as intermediate velocity gas.

Based on maps of the distributions of known intermediate velocity clouds (Wakker & van Woerden 2013), we see that IRC+10216 sightline lies in proximity to the IV Arch intermediate velocity cloud complex. This complex includes gas with velocities in the range $-60 \lesssim V_{\rm LSR} \lesssim -27.5$ km s^{-1} (with the lower negative velocity cutoff being somewhat ambiguous owing to confusion from Galactic emission; Kuntz & Danly 1996). These velocities are comparable to those represented by Component 1 of our GBT spectrum, although based on the results of Kuntz & Danly, the peak column density gas in the IV Arch complex more typically arises ∼10-15 km s^{-1} blueward of the peak column density of Component 1. We conclude that an association between Component 1 and the IV Arch complex is plausible but cannot be made conclusively. Based on the results of Wakker (2001), the distance of the IV Arch complex lies in the range 0.8-1.8 kpc, or at several times the distance of IRC+10216.

REFERENCES

Bergeat, J., Knapik, A., & Rutily, B. 2001, A&A, 369, 178
Blandford, R. & Eicher, D. 1987, Physics Reports, 154, 1
Boothroyd, A. I., Blagrave, K., Lockman, F. J., Martin, R. G., Pinheiro Gonçlaves, D., & Srikanth, S. 2011, A&A, 536, A81
Bowers, P. F. & Knapp, G. R. 1987, ApJ, 315, 305
Bowers, P. F. & Knapp, G. R. 1988, ApJ, 332, 299
Cernicharo, J., Guélin, M., & Kahane, C. 2000, A&AS, 142, 181
Cernicharo, J., Marcelino, N., Agundez, M., & Guélin, M. 2014, A&A, in press (arXiv:1412.1948)
Cohen, M. 1979, MNRAS, 186, 837
Crosas, M. & Menten, K. 1997, ApJ, 483, 913
De Beck, E. et al. 2012, A&A, 539, A108
Decin, L. et al. 2011, A&A, 534, A1
Fong, D., Meixner, M., & Shah, R. Y. 2003, ApJ, 582, L39
Gérard, E., Le Bertre, T., & Libert, Y. 2011, in Why Galaxies Care about AGB Stars II: Shining Examples and Common Inhabitants, ASP Conf. Series, 445, Ed. by F. Kerschbaum, T. Lebzelter, and R. F. Wing (ASP: San Francisco), 329
Glassgold, A. E. & Huggins, P. J. 1983, MNRAS, 203, 517 (GH83)
Greisen, E. W. 2003, Information Handling in Astronomy—Historical Vistas, ed. A. Heck (Dordrecht: Kluwer), 109
Greisen, E. W. 2014, AIPS Memo 118, ftp://ftp.aoc.nrao.edu/pub/software/aips/TEXT/PUBL/AIPSMEM118.PDF
Groenewegen, M. A. T. et al. 2012, A&A, 543, L8
Groenewegen, M. A. T., van der Veen, W. E. C. J., & Matthews, H. E. 1998, A&A, 338, 491
Guelin, M., Forestini, M., Valiron, P., Ziurys, L. M., Anderson, M. A., Cernicharo, J., & Kahane, C. 1995, A&A, 297, 183
Hartmann, D. & Burton, W. B. 1997, Atlas of Galactic Neutral Hydrogen, (Cambridge: Cambridge University Press)
Haud, U. & Kalberla, P. M. W. 2006, Balt. A., 15, 413
Ivezić, Ž. & Elitzur, M. 1996, MNRAS, 279, 1019
Kalberla, P. M. W., Westphalen, G., Mebold, U., Hartmann, D., & Burton, W. B. 1998, A&A, 332, L61
Kendall, T. R., Mauron, N., McCombie, J., & Sarre, P. J. 2002, A&A, 387, 624
Knapp, G. R., Young, K., Lee, E., & Jorissen, A. 1998, ApJS, 117, 209
Kuntz, W. D. & Danly, L. 1996, ApJ, 457, 703
Ladjal, D. et al. 2010, A&A, 518, L141
Lamers, H. J. G. L. M. & Cassinelli, J. P. 1999, Introduction to Stellar Winds, (Cambridge: Cambridge University Press)
Le Bertre, T. & Gérard, E. 2001, A&A, 378, 29
Leão, I. C., de Laverny, P., Mékarnia, D., De Medeiros, J. R., & Vandame, B. 2006, A&A, 455, 187
Levinson, F. H. & Brown, R. L. 1980, ApJ, 242, 416
Mangum, J. G., Emerson, D. T., & Greisen, E. W. 2007, A&A, 474, 697
Martin, D. et al. 2007, Nature, 448, 780
Matthews, L. D., Gérard, E., Johnson, M. C., Le Bertre, T., Libert, Y., & Reid, M. J. 2011, in Why Galaxies Care about AGB Stars II: Shining Examples and Common Inhabitants, ed. F. Kerschbaum, T. Lebzelter, & R. F. Wing, (ASP: San Francisco), 445, 305
Matthews, L. D., Le Bertre, T., Gérard, E., & Johnson, M. C. 2013, AJ, 145, 97
Matthews, L. D., Libert, Y., Gérard, E., Le Bertre, T., Johnson, M. C., & Dame, T. M. 2011, AJ, 141, 60
Matthews, L. D., Libert, Y., Le Bertre, T., Gérard, E., & Reid, M. J. 2008, ApJ, 684, 603
Matthews, L. D. & Reid, M. J. 2007, AJ, 133, 2291 (MR07)
Mauron, N. & Huggins, P. J. 1999, A&A, 349, 203
Mauron, N. & Huggins, P. J. 2010, A&A, 513, A31
Men'shchikov, A. B., Balega, Y., Blöcker, T., Osterbart, R., & Weigelt, G. 2001, A&A, 368, 497
Menten, K., Reid, M. J., Kamiński, T., & Claussen, M. J. 2012, A&A, 543, A73
Morris, M. & Jura, M. 1983, ApJ, 264, 546
Olofsson, H., Johansson, L. E. B., Hjalmarson, Å, & Nguyen-Quang-Rieu 1982, A&A, 107, 128
Osterbart, R., Balega, Y. Y., Blöcker, T., Men'shchikov, A. B., & Weigelt, G. 2000, A&A, 357, 169
Patel, N. et al. 2009, ApJ, 692, 1205
Patel, N. et al. 2011, ApJS, 193, 1
Peek, J. E. G. et al. 2011a, ApJS, 194, 20
Peek, J. E. G., Heiles, C., Peek, K. M. G., Meyer, D. M., & Lauroesch, J. T. 2011b, ApJ, 735, 1
Phillips, J. P., White, G. J., Ade, P. A. R., Cunningham, C. T., Richardson, K. J., Robson, E. I., & Watt, G. D. 1982, A&A, 116, 130
Raymond, J. C., Blair, W. P., & Long, K. S. 1997, ApJ, 489, 314
Reich, P & Reich, W. 1986, A&AS, 63, 205
Ridgway, S. T. & Keady, J. J. 1984, RSPTA, 303, 497
Rodríguez, L. F., Goss, W. M., & Williams, R. 2002, ApJ, 574, 179
Sahai, R. 1990, ApJ, 362, 652
Sahai, R. & Chronopoulos, C. K. 2010, ApJ, 711, L53
Sahai, R. & Nyman, L.-Å. 1997, ApJ, 487, L155
Skinner, C. J., Meixner, M., & Bobrowsky, M. 1998, MNRAS, 300, 29
Stark, R., Dickey, J. M., Burton, W. B., & Wennmacher, A. A&A, 281, 199
Taylor, A. R., Gussie, G. T., & Goss, W. M. 1989, ApJ, 340, 932
Tenorio-Tagle, G., Bodenheimer, P., Różczka, M., & Franco, J. 1986, A&A, 170, 107
Tuthill, P. G., Monnier, J. D., Danchi, W. C., & Lopez, B. 2000, ApJ, 543, 284
van Marle, A. J., Meliani, Z., Keppens, R., & Decin, L. 2011, ApJ, 734, L26
Vassiliadis, E. & Wood, P. R. 1993, ApJ, 413, 641
Verschuur, G. L. & Knapp, G. R. 1971, AJ, 76, 403
Villaver, E., García-Segura, G., & Manchado, A. 2002, ApJ, 571, 880
Villaver, E., Manchado, A., & García-Segura, G. 2012, ApJ, 748, 94
Wakker, B. P. 2001, ApJS, 136, 463
Wakker, B. P. & van Woerden, H. 1991, A&A, 250, 509

Wakker, B. P. & van Woerden, H. 2013, in Planets, Stars, and Stellar Systems Volume 5: Galactic Structure and Stellar Populations, ed. T. D. Oswalt and G. Gilmore (Dordrecht: Springer), 587

Weigelt, G., Balega, Y. Y., Blöcker, T., Hofmann, K.-H, Men'shchikov, A. B., & Winters, J. M. 2002, A&A, 392, 131

Williams, D. R. W. 1973, A&AS, 8, 505

Wood, B. E., Alexander, W. R., & Linsky, J. L. 1996, ApJ, 470, 1157

Young, K., Phillips, T. G., & Knapp, G. R. 1993, ApJS, 86, 517

Zuckerman, B. 1987, in Astrochemistry, IAU Symposium 120, (Reidel: Dordrecht), 345

Zuckerman, B., Terzian, Y., & Silverglate, P. 1980, ApJ, 241, 1014